Contrib Mineral Petrol (2007) 154:191–204
DOI 10.1007/s00410-007-0187-7

ORIGINAL PAPER

Thermochemistry of sulfide liquids III: Ni-bearing liquids at 1 bar

Victor Kress

Received: 25 January 2001 / Accepted: 19 January 2007 / Published online: 29 March 2007

Abstract Experiments were performed in the system O–S–Fe–Ni designed to extend our understanding of the chemistry of sulfide liquids. Results indicate that adding nickel to Fe-rich sulfide liquids in equilibrium with silicate liquids extends their stability field to much higher oxygen fugacities and lower sulfur fugacities. Increasing Ni/Fe at a given temperature and sulfur and oxygen fugacity is accompanied by a significant decrease in the oxygen content of the sulfide liquid. Results of these experiments are combined with data from the literature to calibrate an associated regular solution model for O–S–Fe–Ni liquids. This model represents a complete refit of the associated regular solution model of Kress (Contrib Mineral Petrol 139:316–325, 2000). The resulting model is combined with the olivine solution model of Hirschmann (Am Mineral 76:1232–1248, 1991) to explore the effect of variations in oxygen and sulfur fugacities on the distribution of Fe and Ni between olivine and sulfide liquid. Predicted olivine–sulfide distribution trends parallel those observed by Gaetani and Grove (Geochim Cosmochim Acta 61:1829–1846, 1997), Gaetani and Grove (Earth Planet Sci Lett 169:147–163, 1999), Brenan and Caciagli (Geochim Cosmochim Acta 64:307–320, 2000) and Brenan (Geochim Cosmochim Acta 67:2663–2681, 2003), but are systematically offset toward lower predicted Ni in the sulfide. Nevertheless our results are consistent with the assertion that low K_D^{os} values in magmatic ore deposits such as the J-M Reef reflect high iron contents in the sulfides combined with relatively high oxygen fugacities.

Communicated by T.L. Grove.

V. Kress (✉)
University of Washington Earth and Space Sciences,
Box 351310 Seattle, WA, USA
e-mail: kress@u.washington.edu

Introduction

Sulfide liquids are found in a wide variety of settings on Earth and the terrestrial planets. These liquids are encountered in most igneous rock types where they represent important reservoirs of sulfur, nickel, cobalt and the platinum group elements. The sensitivity of the chemistry and stability field of sulfide liquids to variations in oxygen and sulfur fugacity makes them promising petrogenetic indicators of these important intensive parameters in magmatic systems.

Sulfide liquids in nature are predominantly composed of O, S, Fe, Ni, and Cu in varying proportions. Primary igneous sulfide liquids tend to be dominated by O, S, Fe and Ni, while Cu becomes more dominant in sulfides that have experienced an episode of volatile transport (Luhr 1990), or extended MSS crystallization (Li et al. 1992; Naldrett et al. 1996; Barnes et al. 1997).

In this contribution, we present the results of new equilibration experiments on liquids in the O–S–Fe–Ni system. These data build on experimental data in the O–S–Fe system presented by Kress (1997b). Experimental results are combined with data from the literature to extend and update the associated regular solution model for O–S–Fe liquids of Kress (2000) to apply to liquids in the full O–S–Fe–Ni system.

Experimental technique

Experiments were performed in open silica glass capsules suspended at the hot spot of a vertical quench furnace. The

furnace atmosphere consisted of a controlled mixture of CO_2, SO_2 and H_2, CO_2, CO and SO_2, or SO_2 and H_2. Temperature was measured using an S-type thermocouple in a sealed alumina ceramic sheath. Thermocouples were calibrated several times during the experimental program against the melting point of gold (1,064.43°C). Measured melting temperatures for 99.999% Au ranged from 1,063.5 to 1,064.2°C. The thermocouple was never more than 4 mm from the sample during the experiment. Temperature gradients between the measurement thermocouple and the sample were measured at less than about 0.5°C. Controller drift during the experiment was never larger than 0.8°C.

Gas flow was controlled by carefully calibrated Matson E101 rotameters. Oxygen and sulfur fugacities were calculated using software described in Kress et al. (2004) using thermochemical data from JANAF (Chase et al. 1985). Ebel and Grossmann (2000) pointed out that tabulated values for the Gibbs free energy of formation at T (ΔG_f°) were not consistent with accompanying entropy and enthalpy values for several important species in the JANAF thermochemical compilation used in these gas calculations. Tabulated values for ΔG_f°, Cp°, S° and H°–H_{Tr}° from the two latest JANAF compilations (Chase 1998; Chase et al. 1985) were cross-checked and compared with corresponding values calculated with Shomate equations from the NIST web site (Alfeefy et al. 2001). All values were tested for self-consistency. The Shomate equations were calibrated using data in the latest JANAF compilation (Chase 1998) providing an additional redundant cross-check. All JANAF data used in this study were checked, including the gas species O_2, H_2, S_2, S, S_3, CO, CO_2, SO_2, SO, S_2O, COS, CS, CS_2, H, OH, HO_2, H_2O, H_2O_2, H_2SO_4, H_2S, CH, COH, CH_2, COH_2, CH_3, CH_4, C_2H, C_2H_2, C_2H_4, C_2OH_4, C_2O, C_3O_2, and HS, the liquid species Fe, Ni, Cu and S, and the solid species γFe, δFe, Ni and Cu. Tabulated and calculated values for enthalpies, entropies and heat capacities were found to be consistent within 0.01% for all species. Tabulated ΔG_f° values were consistent with those calculated from tabulated entropy and enthalpy values or calculated from Shomate equations for all species except the gas species S_2O, C_2H_2 and HS. Tabulated values for ΔG_f° at 1000K for the species S_2O, C_2H_2 and HS differ from calculated values by –48, +86 and –50%, respectively. Self-consistent values are tabulated in an earlier JANAF compilation (Stull and Prophet 1971), suggesting that this error was introduced during preparation of the later editions. Unfortunately, the erroneous tabulated ΔG_f° had been used in the gas mixture software described in Kress (1997b). For most gas mixtures considered, calculated oxygen and sulfur fugacities using the corrected ΔG_f° values differ from the original calculated values by less than 1%. For some mixtures, however, the revised values can differ from the original by as much as 0.3 log units in f_{O_2} and 0.7 log units in f_{S_2}. Oxygen and sulfur fugacities for all experiments used in Kress (1997b, 2000) were recalculated using the Shomate equations (Alfeefy et al. 2001).

Gas flow calibration and oxygen fugacity calculations were checked against wüstite-magnetite assemblage indicating a value 0.10 $\log_{10}$ units lower than the electrochemical determination of O'Neill and Pownceby (1993). No correction was made for this minor discrepancy.

The sample suspension device consisted entirely of alumina ceramic, silica glass and Teflon, to avoid reaction with the furnace gas. Experiments were terminated by dropping the sample into a roller-quench apparatus based on the device described in Kress (1997b). This second-generation roller-quench device is considerably improved over the original with roller speeds increased from about 120 rpm to about 2,000 rpm. The increased roller speed produced a dramatic increase in experimental success rate.

Though Kress (1997b) went to considerable lengths to avoid sulfur and water deposition inside the furnace, some deposition was sometimes encountered at the aluminum sample hanger plate at the top of the furnace in very sulfur-rich or hydrogen-rich compositions. This sulfur and water precipitation limited the range of conditions that could be considered in Kress (1997b). The precipitation problem was solved in this study by inserting a 2.4-cm-thick Teflon insulator directly under the aluminum mounting plate. During the experiment, the bottom surface of the Teflon insulator remains well above the condensation temperature of both sulfur and water. A 200°C nichrome-wound heated silica exhaust tube similar to that described by Kress (1997b) was employed to prevent condensation in the exit tube.

Experimental conditions and durations are listed in Table 1. Experiments were equilibrated for between 120 and 337 min. Experimental durations were 3–6 times the minimum required to achieve homogeneous and heterogeneous equilibrium (Kress 1997b). The reported temperature was taken just before quench.

Analytical

Experiments were analyzed with either a JEOL 8900 electron microprobe at the Geophysical Laboratory or a JEOL 7300 at the University of Washington. A 15 kV accelerating potential and 10 nA Faraday current were used on both instruments. Analyses were performed using a 10 μm raster with 30-s counting times. In rare cases the samples proved to be too small to raster the beam, but this had a relatively minor effect on the quality of analyses. Analyses were only performed on grains >10 μm in diameter. Analyses were dropped if totals deviated from 100% by more than 2%, or if Si counts were above back-

Table 1 Experimental conditions

Sample	T (°C)	H_2	CO	CO_2	SO_2	$\log_{10}(f_{O_2})$	$\log_{10}(f_{S_2})$	Time
61	1,251	130	0	110	6	–10.7	–2.95	245
62	1,250	130	0	110	6	–10.71	–2.95	253
64	1,248	200	0	0	6	–13.57	–4.02	263
66	1,248	16	0	10	100	–7.94	–1.58	218
67	1,249	16	0	10	100	–7.93	–1.58	245
68	1,249	16	0	10	100	–7.93	–1.58	235
69	1,248	85	0	100	6	–10.29	–2.46	265
70	1,250	130	0	0	10	–12.58	–3.06	257
70b	1,250	130	0	110	6	–10.71	–2.95	255
71	1,249	130	0	110	6	–10.72	–2.95	239
72	1,248	16	0	10	100	–7.94	–1.58	226
73	1,250	0	100	0	20	–10.67	–1.09	245
74	1,251	0	100	0	20	–10.66	–1.09	289
75	1,251	0	100	0	20	–10.66	–1.09	285
76	1,252	130	0	0	10	–12.56	–3.07	291
77	1,251	130	0	0	10	–12.57	–3.06	308
78	1,249	130	0	0	10	–12.59	–3.07	293
79	1,250	130	0	0	10	–12.58	–3.06	189
80	1,249	16	0	10	100	–7.93	–1.58	337
81	1,250	100	0	30	16	–10.87	–1.95	300
82	1,249	100	0	30	16	–10.88	–1.95	252
83	1,250	100	0	30	16	–10.87	–1.95	331
84	1,250	100	0	30	16	–10.87	–1.95	259
85	1,249	100	0	30	16	–10.88	–1.95	268
87	1,348	175	0	0	10	–11.87	–3.03	247
88	1,349	175	0	0	10	–11.86	–3.02	233
89	1,250	0	140	55	7	–10.84	–1.88	304
91	1,449	175	0	0	10	–10.92	–2.73	195
92	1,450	175	0	0	10	–10.91	–2.73	120
94	1,251	0	140	55	7	–10.83	–1.88	313
96	1,451	175	0	0	10	–10.90	–2.72	228
97	1,349	20	0	108	10	–7.69	–2.65	283
98	1,349	20	0	108	10	–7.69	–2.65	250

Flows are in cm^3/min and durations in minutes

ground. Compositions of experimental products are listed in Table 2. Values in Table 2 represent averages of between 3 and 18 analyses per experiment. 1σ values are based on standard deviation of these analyses. Relatively large standard deviations for oxygen in some of the experiments reflect less effective quenching.

Results

Figure 1 is a plot of oxygen and sulfur contents in liquids equilibrated in the vicinity of 1,250°C, $\log_{10}(f_{O_2}) \approx -10.8$ and $\log_{10}(f_{S_2}) \approx -1.9$. Oxygen contents decrease rapidly with increasing Ni to $X_{Ni}/(X_{Fe} + X_{Ni}) \approx 0.3$, decreasing more slowly with further increase in Ni. This decrease in oxygen with increasing Ni in the sulfide liquid has been observed qualitatively in several studies (Gaetani and Grove 1999; Rose and Brenan 2001; Brenan 2003) Sulfur contents remain roughly independent of Ni-content up to $X_{Ni}/(X_{Fe} + X_{Ni}) \approx 0.5$. At higher Ni-contents, equilibrium sulfur-contents decrease significantly with increasing $X_{Ni}/(X_{Fe} + X_{Ni})$.

Also plotted in Fig. 1 is a single point from Yoshiki-Gravelsins and Touguri (1993) equilibrated under similar conditions. Data from Yoshiki-Gravelsins and Touguri (1993) show trends which are consistent with results from this study, though both oxygen and sulfur-contents in their experiments appear to be biased toward lower values relative to the results of this study under similar conditions. It should be noted that only one of the experiments from

Table 2 Compositions and 1σ estimate for sulfide liquids in wt%

Sample	O	±	S	±	Fe	±	Ni	±
61	5.09	0.32	32.78	0.79	60.09	0.88	1.55	0.15
62	0.99	0.27	30.20	0.34	38.74	0.69	29.22	0.64
64	0.69	0.15	29.11	1.25	33.77	0.93	33.77	1.28
66	1.20	0.17	30.49	0.41	24.84	0.70	42.73	0.70
67	1.59	0.49	30.00	0.84	25.76	1.68	41.68	2.33
68	0.88	0.37	27.67	0.22	11.87	0.63	59.11	0.54
69	2.00	0.78	30.11	1.78	36.31	1.41	30.37	3.66
70	1.07	0.23	32.08	1.06	52.84	1.64	12.97	2.48
70b	1.49	0.15	29.02	0.35	33.97	0.84	35.15	0.81
71	1.31	0.16	29.86	0.38	23.15	1.40	45.53	1.62
72	1.56	0.43	29.19	0.56	21.33	2.06	47.49	2.24
73	1.63	0.33	34.06	0.43	48.97	0.91	15.04	1.04
74	2.06	0.45	32.21	0.70	42.01	1.35	23.15	1.56
75	1.03	0.23	31.20	0.79	22.75	1.89	44.81	2.08
76	1.59	0.97	32.11	1.17	48.19	3.30	17.07	3.40
77	1.13	0.82	30.88	2.45	31.44	3.40	34.92	3.32
78	0.40	0.07	27.14	0.64	16.64	0.36	54.56	0.59
79	0.34	0.09	24.38	0.43	0.15	0.02	74.23	0.41
80	0.24	0.07	27.12	0.76	0.02	0.02	71.58	0.84
81	0.28	0.08	26.81	0.30	0.01	0.01	71.66	0.29
82	0.52	0.34	28.23	0.25	11.66	1.66	58.50	1.46
83	0.29	0.06	26.88	0.41	0.03	0.03	71.83	0.73
84	0.68	0.12	32.01	0.38	40.23	0.83	26.11	0.93
85	1.57	0.73	35.15	0.99	56.21	1.52	6.44	1.52
87	1.69	0.40	29.36	1.22	32.00	1.41	36.18	1.62
88	0.30	0.10	24.03	1.70	0.03	0.03	74.64	1.95
89	0.93	0.52	32.27	0.48	30.38	4.65	35.78	5.58
91	0.79	0.18	25.91	1.01	13.44	0.79	59.10	0.93
94	0.47	0.10	30.98	1.52	25.02	2.93	42.58	4.21
96	0.37	0.14	24.84	1.46	0.08	0.04	73.80	1.34
97	0.67	0.16	27.01	0.69	13.46	0.37	58.09	0.45
98	0.26	0.08	24.49	0.18	0.03	0.03	74.51	0.19

Each composition is an average of between 3 and 18 individual analyses

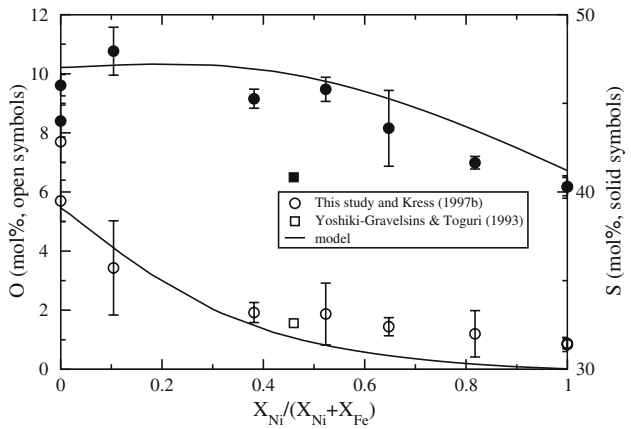

Fig. 1 Plot of oxygen and sulfur contents of sulfide liquids equilibrated at about 1,250°C, $\log_{10}(f_{O_2}) \approx -10.8$ and $\log_{10}(f_{S_2}) \approx -1.9$ plotted against molar $X_{Ni}/(X_{Ni} + X_{Fe})$. *Solid line* is calculated using model from this study

Yoshiki-Gravelsins and Touguri (1993) was plotted in Fig. 1 merely because this was the only point from their study that was directly comparable to this particular set of experiments. The compositional offset displayed in this figure is typical of other points from this study.

Equilibrium sulfur-content decreases less strongly with increasing $X_{Ni}/(X_{Fe} + X_{Ni})$ at low sulfur fugacities. At $\log_{10}(f_{O_2}) \approx -10.8$ and $\log_{10}(f_{S_2}) \approx -3$ equilibrium sulfur-content is approximately independent of melt Ni-content (Fig. 2). Even under these conditions, however, oxygen-content decreases significantly with increasing $X_{Ni}/(X_{Fe} + X_{Ni})$.

Figure 3 is a plot of $(X_{Fe} + X_{Ni}) - (X_O + X_S)$ versus $X_{Ni}/(X_{Fe} + X_{Ni})$ for the same experiments plotted in Fig. 1. The ratio of cations to anions in the sulfide increases substantially with increasing $X_{Ni}/(X_{Fe} + X_{Ni})$. This trend was observed at all temperatures, oxygen fugacities and sulfur-

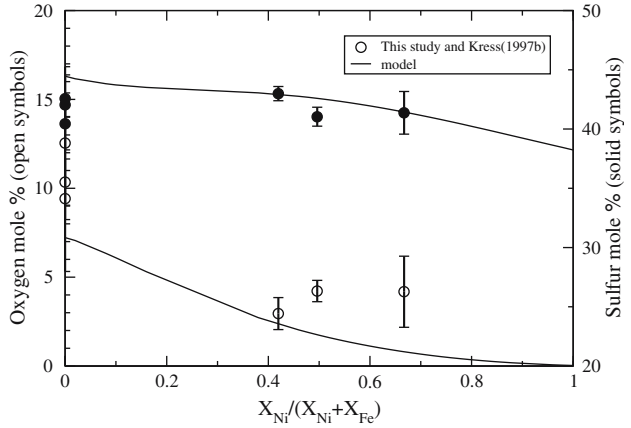

Fig. 2 Plot of oxygen and sulfur contents of sulfide liquids equilibrated at about 1,250°C, $\log_{10}(f_{O_2}) \approx -10.8$ and $\log_{10}(f_{S_2}) \approx -3$ plotted against molar $X_{Ni}/(X_{Ni} + X_{Fe})$. *Solid line* is calculated using model from this study

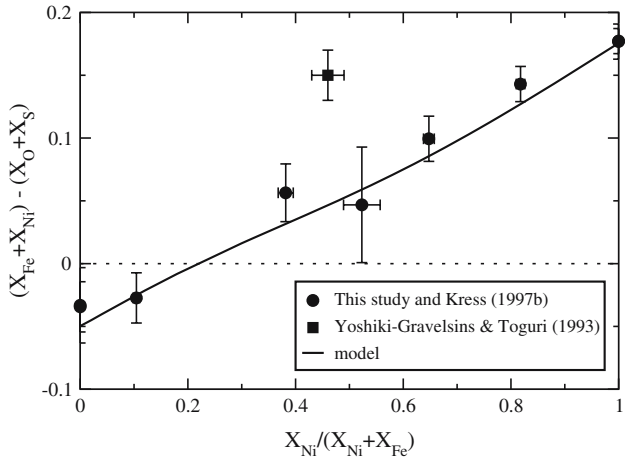

Fig. 3 Plot of molar $(X_O + X_S) - (X_{Fe} + X_{Ni})$ versus $X_{Ni}/(X_{Ni} + X_{Fe})$ for experiments equilibrated at 1,250°C, $\log_{10}(f_{O_2}) \approx -10.8$ and $\log_{10}(f_{S_2}) \approx -1.9$. *Solid line* is calculated using model from this study

fugacities explored in this study. If O, S, Fe, and Ni were all divalent in the sulfide liquid, then $(X_{Fe} + X_{Ni}) - (X_O + X_S)$ would be zero. Assuming that these are dominantly ionic liquids, deviations from zero will reflect a non-divalent component among anions, cations or both. Kress (1997b) observed that Fe < O + S for liquids in the O–S–Fe system equilibrated over a wide range of temperatures, oxygen and sulfur fugacities. Kress (1997b) attributed this to a significant ferric iron component in sulfide liquids. With increasing $X_{Ni}/(X_{Fe} + X_{Ni})$, $(X_{Fe} + X_{Ni}) - (X_O + X_S)$ increases to positive values. Cation excess in Ni-rich sulfide liquids suggests that metallic nickel, or less likely sulfite, may be an important species in these liquids.

Kress (1997b) observed that sulfide liquids are not stable in equilibrium with a quartz-saturated silicate liquid in the O–S–Fe–Si system at high oxygen fugacities or low sulfur fugacities. This sulfide-stability boundary in the Ni-free system is labeled ''0.0'' in Fig. 4. Results from this study suggest that adding Ni to the sulfide liquid increases the stability field of sulfide liquids to higher oxygen fugacities and lower sulfur fugacities as indicated in Fig. 4. The Ni/Fe ratio in sulfides may, therefore, be used to place bounds on magma redox state and sulfur fugacity in magmatic systems. The exact position of these stability boundaries will vary somewhat with silicate liquid composition. Quantitative application of this oxy/sulfur geobarometer in natural systems will, therefore, require self-consistent thermodynamic models for sulfide and silicate liquids. Nevertheless, important qualitative conclusions can be drawn from the stability relations displayed in Fig. 4.

If one takes an Fe-rich sulfide liquid initially equilibrated with a silicate liquid under reducing conditions into a more oxidizing environment, Fe in the sulfide will react with the silicate. The total amount of sulfide liquid will decrease, and the residual sulfide will be enriched in Ni. This may be an important mechanism for Ni enrichment in magmatic ore bodies.

The breakdown of sulfides in the presence of a silicate melt can be described by a reaction of the form:

$$\mathrm{FeS}^{\mathrm{sulf.liq.}} + \frac{1}{2}\mathrm{O}_2 \rightleftharpoons \mathrm{FeO}^{\mathrm{sil.liq.}} + \frac{1}{2}\mathrm{S}_2. \quad (1)$$

Under conditions more reducing than that defined by the Ni–NiO assemblage, sulfur dissolves in the silicate primarily as sulfide according to a reaction analogous to:

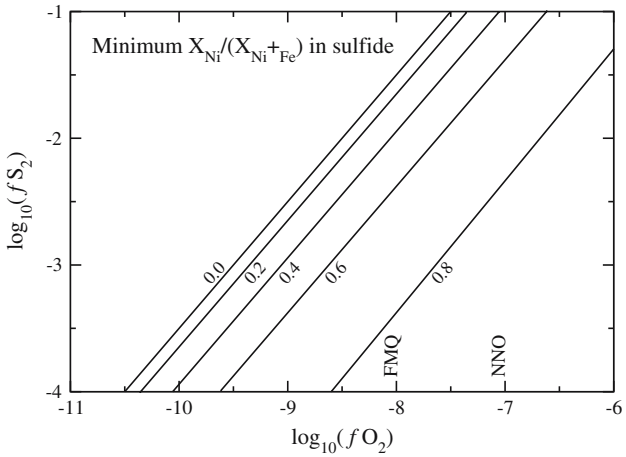

Fig. 4 Approximate boundary of conditions under which sulfide liquids are stable in equilibrium with silicate liquids in O–S–Fe–Ni–Si experiments at 1,250°C as a function of molar $X_{Ni}/(X_{Ni} + X_{Fe})$ based on experiments from this study and Kress (1997b). Sulfide liquids are stable only on *upper left side* of appropriate *diagonal line*. Approximate positions of fayalite–magnetite–quartz (FMQ) and nickel–nickel oxide (NNO) buffers are shown for reference

$$2S^{2-}_{(silicate)} + O_2 \rightleftharpoons 2O^{2-}_{(silicate)} + S_2 \quad (2)$$

(e.g. Carroll and Rutherford 1985; Katsura and Nagashima 1974; Fincham and Richardson 1954; Nagashima and Katsura 1973). Comparing Eqs. 1 and 2, it is clear that, as long as silicate and sulfide melts coexist, increases in oxygen fugacity will generate a consequent increase in sulfur fugacity until the sulfide is exhausted. This will drive the liquid toward the upper right in Fig. 4. If the silicate liquid is undersaturated with respect to a vapor phase, the increase in sulfur fugacity will tend to drive it toward vapor saturation. If it is already saturated with a vapor phase, this vapor phase will tend to buffer further increases in sulfur fugacity. Thus, under vapor-saturated conditions a given change in oxygen fugacity will result in a greater degree of sulfide breakdown than a similar change under the vapor-absent case. Kress (1997a) proposed oxidation of a sulfide-saturated basalt as a mechanism for rapidly liberating on the order of 45% of the total SO_2 emitted during the June 1991 eruption of Pinatubo. In this case, oxidation of the basalt was a consequence of magma mixing with the oxidized dacite which dominated this eruptive event.

Mavrogenes and O'Neill (1999) and O'Neill and Mavrogenes (2002) suggested, on the basis of theoretical analysis, that the sulfur content of silicate liquid at sulfide saturation (SCSS) will depend on T and P, but not on f_{O_2} or f_{S_2}. The flaw with this argument lies in their neglect of ferric iron in the silicate liquid. Neglecting ferric/ferrous equilibrium in the silicate, the activity of FeO in the silicate liquid becomes entirely independent of f_{O_2}. O'Neill and Mavrogenes (2002) also make the more qualified and reasonable assumption that the effect of dissolved oxygen on the activity of FeS in the sulfide liquid is negligible to first order. With both $a^{\text{sil. liq.}}_{FeO}$ and $a^{\text{sulf. liq.}}_{FeS}$ assumed to be independent of f_{O_2}, oxygen drops out of the sulfide–silicate reaction, leading to the erroneous conclusion that SCSS is independent of oxygen fugacity. When reaction to ferric iron in the silicate is considered, it is evident that increasing f_{O_2} will decrease $a^{\text{sil. liq.}}_{FeO}$. Lower $a^{\text{sil. liq.}}_{FeO}$ will deplete iron in the coexisting sulfide liquid and sulfur fugacity must increase to maintain saturation. Considering O'Neill and Mavrogenes (2002) Eq. 24, therefore, an increase in f_{O_2} with forced saturation with sulfide will lead to an increase in both f_{S_2} and SCSS.

Arguments regarding sulfide–silicate and sulfide–vapor equilibrium to natural systems must remain qualitative as long as we lack a quantitative thermochemical model for all relevant phases. In the following section we use experimental data to revise and extend the associated regular solution model for O–S–Fe liquids from Kress (2000) to apply in nickel-bearing sulfide liquids.

Associated regular solution model for sulfide liquid phase

Kress (1997b) noted that the Gibbs mixing surface of sulfide liquids in the O–S–Fe system exhibited features that were extremely difficult to fit using the standard asymmetric regular solution formulation. Kress (1997b) encountered particular problems in fitting the Fe–O join due to the presence of a large region of liquid immiscibility between metal and oxide liquids coupled with rapid changes in component potentials over a restricted range of melt compositions at higher oxygen contents. This led Kress (2000) to propose an associated regular solution formulation which reproduces experimental results well. This formulation assumes homogeneous equilibrium between M species in an N component solution, where $M \geq N$. Mixing between the M species is represented by a regular solution form, where most binaries are assumed to be symmetric and ternary terms are ignored.

Species stoichiometries were chosen according to a variety of criteria. Some stoichiometries were chosen on the basis of pronounced inflections activity-composition plots, reflecting rapid rise in chemical potentials over restricted composition range. In many cases, species were added where large negative Margules parameters were encountered during the fitting procedure. In such cases, the exact position of the species might then be refined by systematics in the residuals, or by analogy with stable solids. Hypothesized species were deleted if their formation energies were driven positive in the fitting process. In other cases, several candidate species would be added and allowed to self-select via the fitting process. Only relatively simple charged balanced stoichiometries were considered.

In the model proposed in this study, we assume liquids in the four-component O–S–Fe–Ni system to be made up of the 11 species O, S, Fe, Ni, FeO, $FeO_{1.5}$, FeOS, FeS, NiO, NiS, and $Ni_{0.25}S_{0.25}O$. These 11 species are related by the seven homogeneous speciation reactions:

$$Fe^{\ell} + O^{\ell} \rightleftharpoons FeO^{\ell} \quad (3)$$

$$Fe^{\ell} + \frac{3}{2}O^{\ell} \rightleftharpoons FeO^{\ell}_{1.5} \quad (4)$$

$$Fe^{\ell} + O^{\ell} + S^{\ell} \rightleftharpoons FeOS^{\ell} \quad (5)$$

$$Fe^{\ell} + S^{\ell} \rightleftharpoons FeS^{\ell} \quad (6)$$

$$Ni^{\ell} + O^{\ell} \rightleftharpoons NiO^{\ell} \quad (7)$$

$$Ni^{\ell} + S^{\ell} \rightleftharpoons NiS^{\ell} \quad (8)$$

$$\frac{1}{4}Ni^{\ell} + \frac{1}{4}S^{\ell} + O^{\ell} \rightleftharpoons Ni_{0.25}S_{0.25}O^{\ell}, \quad (9)$$

Where the superscripted ℓ emphasizes that these are homogeneous species in the sulfide liquid phase.

The Gibbs free energy (G) of the liquid can be expressed as a Margules expansion truncated at third order (Thompson 1967):

$$G = \sum_{i}^{m} n_i \mu_i + \sum_{i}^{m} n_i RT \ln(X_i) + N \sum_{i}^{m} \sum_{j}^{m} \sum_{k}^{m} W_{ijk} x_i j x_k, \quad (10)$$

where n_i, x_i and μ_i are moles, mole fraction, and chemical potential of *species i*, respectively and N is total moles. W are asymmetric Margules parameters. For the sake of simplicity, W_{ijk}, where $i \neq j \neq k$ or $i = j = k$ are assumed to be zero. This allows us to express all Margules parameters in simpler two-term notation ($W_{ij} = W_{ijj}$). The degree to which Margules terms have physical/chemical significance beyond being mere fit parameters is an expression of how well species stoichiometries have been chosen. In general, positive interaction parameters may express real unfavorable mixing energies between melt species. The interpretation of negative Margules parameters is more ambiguous, probably reflecting inappropriate choice of species stoichiometries. A more complete development of the associated regular solution form along with a robust algorithm for estimating equilibrium speciation are presented in Kress (2000, 2003).

Standard states for liquid Fe and Ni and S are adopted from JANAF Thermochemical tables (Chase et al. 1985). All other values were estimated based on weighted nonlinear least-squares regression of all available high-quality experiments (Gill and Murray 1978). Standard states are relative to the stable element at 1,300 K.

The thermodynamic mixing model we seek to constrain contains 116 potential-fitted variable values. In practice, however, only 48 of these variables were found to have significant effect on residuals (see Tables 3, 4).

Table 3 Regressed thermodynamic values for Ni-bearing sulfide liquids

Species	μ_{1300}° (J)	$\bar{s}_{1300}$ (J)
O	44,049	65.94
FeO	–179,389	135.34
$FeO_{1.5}$	–232,521	148.94
NiO	–72,035	191.97
FeS	–93,139	130.580
NiS	–51,452	186.76
FeOS	–153,852	390.91
$Ni_{0.25}S_{0.25}O$	–59,398	397.65

Standard states are relative to the stable elements at 1,300 K

One necessary condition for stability in any solution is that the matrix formed by the second derivative of the Gibbs free energy with respect to components (the Gibbs Hessian) must be positive-definite (e.g. Kress 2003; Gibbs 1961, p. 111). The Gibbs Hessian is positive-definite if all of its eigenvalues are positive. In fitting a complicated solution by equating chemical potentials alone, it is possible to achieve an excellent fit in terms of chemical potentials where significant portions of the solution are not stable in the thermodynamic sense. To prevent this, we create an additional least-squares constraint for each experimental composition that increases monotonically as the smallest eigenvalue falls below a given positive threshold value. This creates a least squares penalty that will tend to drive the Gibbs–Hessian definitively positive-definite in the fitting process. A positive-definite Hessian indicates that a given point in composition space is outside the spinodal. Strictly speaking, this is not a sufficient condition for stability of a given composition. With sufficiently complete experimental coverage, however, erroneous regions of immiscibility can easily be avoided. As an additional benefit, this additional constraint on the shape of the free energy surface significantly improves the robustness and viability of the fit.

Combining phase equilibrium and phase stability constraints, a total of 1,843 equations were formed from 1,226 experiments. Variable values for the O–S–Fe system are revised from those presented in Kress (2000) to reflect corrected gas compositions, improvements in the fitting software and the addition of stability constraints.

The thermochemistry of liquids in the Fe–Ni binary has been studied by a number of workers (Conard et al. 1978; Chuang et al. 1986a, b; Larrain 1980; Tomiska 1985; Tomiska and Neckel 1985; Bristow 1939; Hanson and Freeman 1923). Figure 5 shows Knudsen cell determination of the excess Gibbs free energy of mixing in Fe–Ni liquid alloys at 1,600°C. Results from Zellars et al. (1959), Conard et al. (1978) and Rammensee and Fraser (1981) are in good agreement. Results of Tomiska (1985) indicate a somewhat smaller negative deviations from ideality than the other studies. Tsemekhman and Vaisburd (1969) present data in iron redox state in Fe–Ni–O liquids, however, they do not present either experimental methods or analytical techniques and these data were not considered in fitting. Vaisburd et al. (1969) present a graphical representation of their model for S–Fe–Ni liquids based on EMF data, however, neither the model, the data, nor details of the experiment are presented. These data were also omitted from the fit.

The asymmetric regular solution fit for the Fe–Ni binary from this study is represented by the solid line in Fig. 5. Though associated regular solution models have been

Table 4 Regular solution values for Ni-bearing sulfide liquids

	S	Fe	Ni	FeO	$FeO_{1.5}$	NiO	FeS	NiS	FeOS	$Ni_{0.25}S_{0.25}O$
S	0	0	0	0	0	0	–21,971	46,930	44,201	19,444
Fe	"	0	–13,720	69,049	26,016	46,726	11,098	–34,811	–3,438	0
Ni	"	–6,102	0	185,737	104,123	46,861	–11,389	–71,588	159,666	–67,300
FeO	"	87,503	"	0	–21,712	–60,040	0	0	0	0
$FeO_{1.5}$	"	36,221	"	–10,871	0	0	0	0	0	0
NiO	"	"	"	"	"	0	0	2,931	0	0
FeS	40,100	"	"	"	"	"	0	–14,791	16,077	0
NiS	"	"	–7,105	"	"	"	–9,191	0	0	49,009
FeOS	"	"	"	"	"	"	–71,847	"	0	0
$Ni_{0.25}S_{0.25}O$	"	"	"	"	"	"	"	"	"	0

Values are in Joules. Double quotes indicate that value is identical to that of symmetric pair

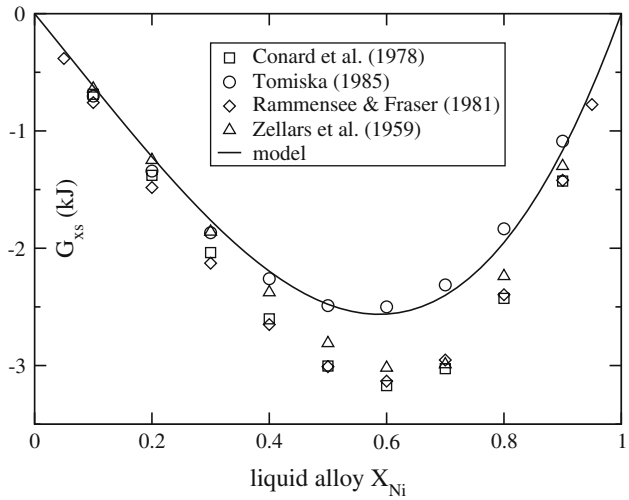

Fig. 5 Plot of mixing excess energy across Fe–Ni join at 1,600°C. Data are from Conard et al. (1978), Tomiska (1985), Rammensee and Fraser (1981) and Zellars et al. (1959). *Solid line* is calculated using model from this study

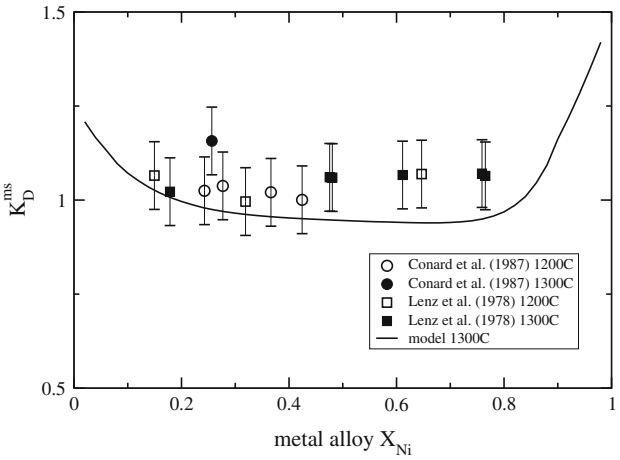

Fig. 6 Comparison of calculated and experimental metal sulfide plotted against Ni in metal alloy. Experimental data are from Conard et al. (1987) and Lenz et al. (1978). The model curve is calculated at 1,300°C using the solid metal alloy model of Tomiska and Neckel (1985). Errors are based on assumed 4% relative analytical uncertainty

proposed for liquids in this binary (Chuang et al. 1986b; Larrian 1980), the added complexity of including an associated melt species along the Fe–Ni join was judged to be unjustified. It is interesting to note that the final fit more closely reproduces the data of Tomiska (1985) than those of Zellers et al. (1959), Conard et al. (1978) and Rammensee and Fraser (1981). This is true even if the data of Tomiska (1985) are omitted from the fit. The model derived in this study reproduces the Fe–Ni alloy–liquid phase diagram to well within the experimental constraints when used with the corresponding solid alloy model of Tomiska and Neckel (1985).

Experimental data for distribution of Fe and Ni between coexisting solid metal alloy and sulfide liquid are presented in Fig. 6. Figure 6 is a plot of K_D^{ms} versus Ni in the solid alloy, where:

$$K_D^{ms} \equiv \frac{X_{\mathrm{Fe}}^{\mathrm{metal}} X_{\mathrm{NiS}}^{\mathrm{sulfide\ liquid}}}{X_{\mathrm{Ni}}^{\mathrm{metal}} X_{\mathrm{FeS}}^{\mathrm{sulfide\ liquid}}}. \quad (11)$$

Experimental values are independent of Ni content in the alloy within estimated uncertainty. If one assumes that oxygen in the sulfide is negligible, sulfide-metal equilibrium at fixed T and P is a completely determined problem. The solid line in Fig. 6 is calculated based on the models of Tomiska and Neckel (1985) and this study. Sulfur fugacity is allowed to float in these calculations, but remains remarkably constant around $\log_{10}(f_{S_2}) \approx -5.5 \pm 0.3$ across the binary. The calculated curve is biased between zero and about 625 J below the experimental values.

Nickel–sulfide liquids are employed in extracting Ni from ore in the top-blown rotary converter process. For this

reason, experimental data on the Ni–S binary are plentiful and of high quality (Meyer et al. 1975; Nagamori and Ingraham 1970; Rosenqvist 1954; Cemic and Kleppa 1986). Experiments in the Ni–S binary are considerably more self-consistent than experiments in iron-bearing sulfides. This is probably due to the fact that nickel sulfide liquids are inert relative to a wider variety of crucible and sampling materials than their iron-bearing counterparts. Figure 7 is a plot of sulfur fugacity versus sulfur content for a subset of these experiments equilibrated close to 1,000, 1,200, 1,400 and 1,600°C. The rapid rise in sulfur fugacity as NiS stoichiometry is approached is consistent with our choice of NiS melt species. Interaction terms between Ni and NiS species are large, negative and asymmetric. This negative interaction enthalpy between Ni and NiS species hints at the existence of yet another melt species of intermediate stoichiometry. Incorporation of a melt species with Ni_2S stoichiometry resulted in a fit to this binary as good as that presented in Tables 3 and 4. Unfortunately, in order to achieve the same quality of fit, this model replaced two Ni–NiS interaction variables with W_{Ni,Ni_2S} and two standard state variables. Thus, addition of the Ni_2S species added one variable and slowed calculation of homogeneous equilibrium without improving the quality of the fit significantly. The added complexity was judged to be unjustified, and the Ni_2S species was omitted from the final fit.

Kullerud and Yund (1962) explored liquid immiscibility at the sulfur-rich side of the Ni–S binary. These data were used to constrain the positive symmetric NiS–S mixing

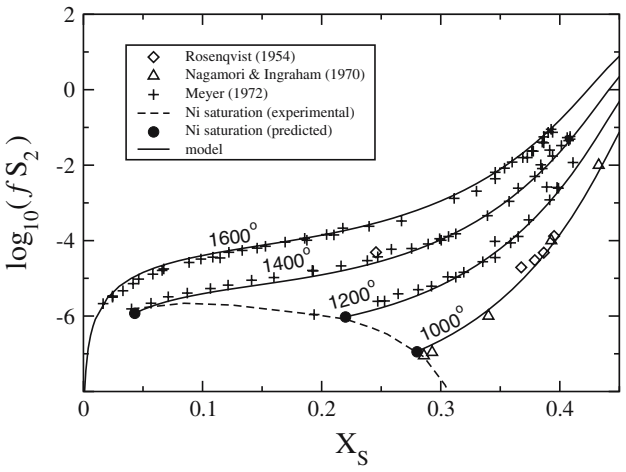

Fig. 7 Plot of sulfur fugacity for sulfide liquids on the Ni–S binary at 1,000, 1,200, 1,400 and 1,600°C. Experimental data are from Rosenqvist (1954), Nagamori and Ingraham (1970) and Meyer (1972). For clarity, only experiments within 5 of 1,000, 1,200, 1,400 and 1,600°C are shown. The *dashed line* indicates experimentally determined polythermal Ni metal saturation surface (Nagamori and Ingraham 1970; Meyer 1972), truncated by the 1,453° Ni melting temperature. *Solid lines* are predicted from this study

value in Table 4. For consistency, similar liquid immiscibility data from Kullerud (1961) in the Fe–S binary were used to refine the fit of Kress (2000) for the O–S–Fe ternary. The resulting fit is substantially better, but includes three new mixing variables not included in the original O–S–Fe fit (Kress 2000).

At least three other thermodynamic models have been proposed for the Ni–S liquids (Meyer et al. 1975; Nagamori and Ingraham 1970; Sharma and Chang 1980; Kellogg 1976). These thermodynamic models are all fitted to essentially the same experimental data set and all reproduce the experimental data with good fidelity. The model of Meyer et al. (1975) is based on a 12-term power series expansion which is incompatible with the regular solution adopted in this study. The model of Kellogg (1976) uses the species NiS as the sulfur-rich component, and is therefore difficult to adapt directly to the O–S–Fe–Ni quaternary. The functional form of the model of Nagamori and Ingraham (1970) is incompatible with the form adopted in this study. The model of Sharma and Chang (1980) is of a compatible form; however, the Sharma and Chang (1980) model involves ten separate fitted variables including four excess entropy of mixing terms. In contrast, the model presented here requires only five fitted variables relevant to the Ni–S binary to achieve roughly the same quality of fit on the Ni-rich side of the binary and a superior fit on the S-rich side of the binary.

Experimental data in the O–S–Fe–Ni quaternary are limited to this study and that of Yoshiki-Gravelsins and Toguri (1993). Compositional trends observed in these two studies are consistent; however, liquid anion contents reported in Yoshiki-Gravelsins and Toguri (1993) are consistently lower than those observed in liquids equilibrated under similar conditions from this study. This discrepancy could be the result of slower quench rate in the Yoshiki-Gravelsins and Toguri (1993) experiments, analytical bias between the two studies or both. Experiments of Yoshiki-Gravelsins and Toguri (1993) were not incorporated in the final fit.

Experiments in the O–S–Fe–Ni system from this study are compared with model predictions in Figs. 1, 2 and 3. Though minor systematic errors appear along particular slices of $T - X - f_{O_2} - f_{S_2}$ space, the model does a consistently good job of reproducing a wide variety of experimental constraints from a diverse group of laboratories. Model errors are generally smaller than differences between the results of experiments from different laboratories. Inter-laboratory error is likely to be responsible for most of the minor systematic errors. Nevertheless, data were dropped from the fit only where obvious problems in experimental design were documented. The model presented here represents all of the resolvable trends in the data and serves as a solid thermodynamic basis for pre-

dicting the chemistry of sulfide liquids in equilibrium with other magmatic phases.

Fe–Ni exchange between olivine and sulfide liquid

Partitioning of iron and nickel between coexisting olivine and sulfide liquids has long been recognized as a potentially useful indicator of magmatic conditions in igneous rocks. This partitioning is commonly expressed in terms of a ''distribution coefficient'' K_D^{os}, where

$$K_D^{os} \equiv \frac{X^{\text{olivine}}_{\text{FeSi}_{0.5}\text{O}_2} X^{\text{sulfide liquid}}_{\text{NiS}}}{X^{\text{olivine}}_{\text{NiSi}_{0.5}\text{O}_2} X^{\text{sulfide liquid}}_{\text{FeS}}}. \quad (12)$$

Several experimental studies have explored the dependence of K_D^{os} on temperature, oxygen and sulfur fugacity and composition both in evacuated silica capsules (Fleet et al. 1977, 1981; Fleet and MacRae 1987, 1983; Clark and Naldrett 1972), and under controlled fugacity conditions (Duke and Naldrett 1978; Boctor 1981; Peach and Mathez 1993; Fleet 1989; Fleet and MacRae 1988; Gaetani and Grove 1997, 1999; Brenan and Caciagli 2000; Brenan 2003). Only five of the controlled fugacity experiments (Peach and Mathez 1993; Gaetani and Grove 1997, 1999; Brenan and Caciagli 2000; Brenan 2003) explicitly account for oxygen in the sulfide phase. Comparison of sulfide compositions from those studies with more rapidly quenched experiments from this study indicate that measured S and O contents in their sulfides have partially reset during quench. However, assuming adequate re-integration of quench products in the above experiments, it is unlikely that K_D^{os} has been substantially altered during quench.

Boctor (1981, 1982) measured f_{O_2} -dependent values for K_D^{os}, ranging from 8.2 to 15.4. Fleet et al. (1977, 1981) and Fleet and MacRae (1987, 1983) measured higher K_D^{os} values ranging from about 30 to 35. Results from the latter group suggest that Fe–Ni partitioning between sulfide melts and olivine is essentially independent of temperature, pressure, oxygen fugacity and sulfur fugacity over a wide range.

In a more recent study, Brenan and Caciagli (2000) found that K_D^{os} increases significantly with increasing weight percent Ni in the sulfide. They found that K_D^{os} decreases with increasing oxygen fugacity and is roughly independent of sulfur fugacity. These results were refined and amplified in a later work (Brenan 2003). To explore this issue more completely, the thermodynamic model presented in this study can be combined with the olivine thermochemical model from Hirschmann (1991) to calculate K_D^{os} both under experimental conditions and under conditions that resist experimental exploration.

Figure 8 compares K_D^{os} predicted from the model with experimental data as a function of Ni-content of the sulfide at 1,300°C, $\log_{10}(f_{O_2}) \approx -9$ and $\log_{10}(f_{S_2}) \approx -1.7$. For the solid line, olivine was fixed at fo_{90} with fayalite and Ni–olivine allowed to adjust to equilibrium with the coexisting sulfide. Both model and experiments show an increase in K_D^{os} with increasing Ni in the sulfide. In this plot, the model predicts K_D^{os} values between 0.3 and 1.1 ln units lower than experimental data under similar conditions and forsterite content indicate, corresponding to between 2 and 7 kJ of error. This compares with 4kJ of scatter in experiments from Brenan and Caciagli (2000) performed under nearly identical conditions. The average model error for all K_D^{os} experiments considered is –0.6 kJ with a standard deviation of 4.4 kJ.

Olivines from Brenan and Caciagli (2000) range in forsterite-content from fo_{47} to fo_{92}; so it is useful to explore the effect of forsterite component in the olivine on calculated K_D^{os}. The dashed line in Fig. 8 was calculated for equilibrium with fo_{80} olivine. Decreasing forsterite in the olivine increases K_D^{os}, and this effect increases slightly with increasing Ni. This forsterite-dependence is not responsible for the experimental scatter in Fig. 8, as the plotted experimental olivines only range from fo_{87} to fo_{92} and the highest K_D^{os} is from a fo_{88} experiment. Similarly, variations in oxygen and sulfur fugacities in the experiments plotted in Fig. 8 are not perfectly correlated with K_D^{os}, though these variations may contribute to the experimental scatter in this plot.

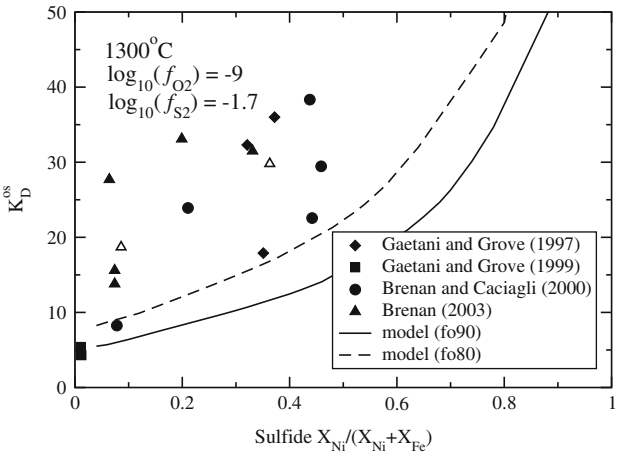

Fig. 8 Predicted K_D^{os} as a function of $X_{Ni}/(X_{Ni} + X_{Fe})$ in the sulfide at 1,300°, $\log_{10}(f_{O_2}) \approx -9$ and $\log_{10}(f_{S_2}) \approx -1.7$. Experiments of Gaetani and Grove (1997), Gaetani and Grove (1999), Brenan and Caciagli (2000) and Brenan (2003) span $\log_{10}(f_{O_2}) \approx -8.6$ to –9.5 and $\log_{10}(f_{S_2}) \approx -1.6$ to –1.7. Gaetani and Grove experiments are at 1,350°C, while experiments from Brenan lab were performed at 1,300°C. *Solid symbols* represent experiments with $fo_{87\text{-}92}$ olivines. *Open symbols* span $fo_{75\text{-}78}$. Olivine potentials were calculated using the model of Hirschmann (1991). The *solid curve* was calculated for fo_{90} olivine while the *dashed curve* was calculated for fo_{80} olivine

K_D^{os} is plotted against $\log_{10}(f_{O_2})$ in Fig. 9. The model curve is calculated for equilibrium with olivine at 1,300°C and $\log_{10}(f_{S_2}) = -1.7$ with sulfide composition fixed at $X_{Ni}/(X_{Ni} + X_{Fe}) = 0.5$. The model predicts a decrease in K_D^{os} with increasing $\log_{10}(f_{O_2})$ parallel to that observed by Brenan and Caciagli (2000). As in Fig. 8, the model curve lies somewhat lower than the experiments would indicate. Decreasing forsterite-content increases the predicted value for K_D^{os}, and the magnitude of this effect increases slightly with decreasing f_{O_2}. The calculated effect of oxygen fugacity on K_D^{os} becomes significantly larger as the sulfides become more iron-rich.

Figure 10 is a plot of K_D^{os} against $\log_{10}(f_{S_2})$ at fixed temperature, oxygen fugacity and $X_{Ni}/(X_{Ni} + X_{Fe}) = 0.5$. The curve calculated at $\log_{10}(f_{O_2}) = -9$ corroborates the experimental observation (Brenan and Caciagli 2000) that K_D^{os} is only mildly dependent on sulfur fugacity under these conditions.

The dashed curve in Fig. 10 is calculated under identical conditions except $\log_{10}(f_{O_2}) = -10.5$. These results indicate that the effect of sulfur fugacity on K_D^{os} increases with decreasing oxygen fugacity. Put another way, the predicted effect of oxygen fugacity on K_D^{os} is more pronounced at lower sulfur fugacity.

Though the sulfide liquid model from this study appears to represent all of the major trends observed in experimental studies of olivine–sulfide equilibrium, the apparent bias toward lower K_D^{os} is troubling. It does not seem to be possible to derive a sulfide model that is faithful to the experimental constraints, using the best-published models

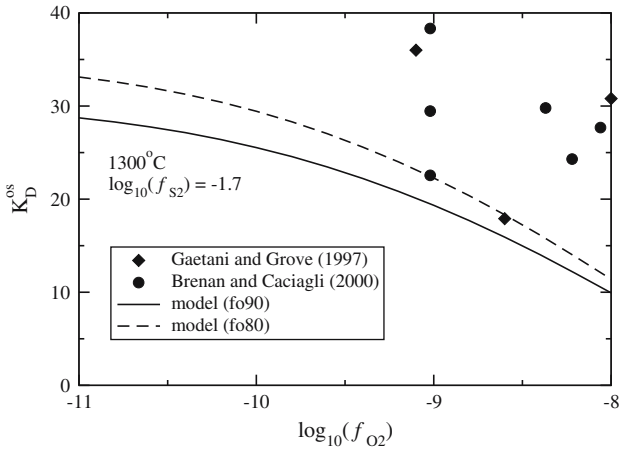

Fig. 9 K_D^{os} versus $\log_{10}(f_{O_2})$ for experiments equilibrated at 1,300°C, $\log_{10}(f_{S_2}) \approx -1.7$ with $X_{Ni}/(X_{Ni} + X_{Fe}) \approx 0.5$. Experiments of Gaetani and Grove (1997), and Brenan and Caciagli (2000) range from $\log_{10}(f_{S_2}) \approx -1.5$ to -1.8 and $X_{Ni}/(X_{Ni} + X_{Fe}) \approx 0.35$ to 0.65. Gaetani and Grove (1997) experiments are at 1,350°C, while Brenan and Caciagli (2000) experiments were performed at 1,300°C. Experimental olivines span $fo_{85\text{-}92}$. Olivine potentials were calculated for fo_{90} composition using model from Hirschmann (1991)

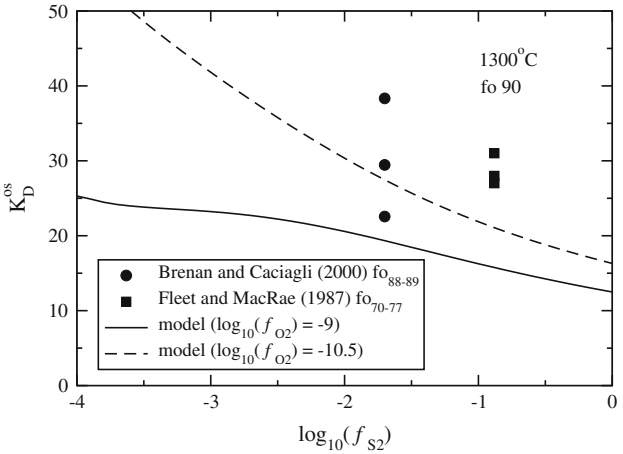

Fig. 10 K_D^{os} versus $\log_{10}(f_{S_2})$ for experiments equilibrated at 1,300° with $X_{Ni}/(X_{Ni} + X_{Fe}) \approx 0.5$. Experimental $X_{Ni}/(X_{Ni} + X_{Fe})$ range from 0.44 to 0.59. Experiments and the *solid curve* are at $\log_{10}(f_{O_2}) \approx -9$ while the *dashed curve* was calculated at $\log_{10}(f_{O_2}) \approx -10.5$. Experimental olivines from Brenan and Caciagli (2000) span $fo_{88\text{-}89}$ while those of Fleet and MacRae (1987) range from $fo_{70\text{-}77}$. Our results suggest that K_D^{os} of Fleet and MacRae (1987) would have been somewhat lower had they been performed with more forsteritic olivines. Olivine potentials were calculated for fo_{90} composition using model from Hirschmann (1991)

for olivine and solid alloy. Higher weighting on K_D^{os} data improves the fit to these data, but correspondingly increases residuals in metal–sulfide, sulfide–gas and metal–oxide experiments.

Figure 11 is a plot of ΔG for the reaction $NiSi_{0.5}O_2 + Fe \rightleftharpoons FeSi_{0.5}O_2 + Ni$ versus mole fraction Ni–olivine for one-bar experimental compositions from Snyder and Carmichael (1992) and Campbell et al. (1979) calculated using the olivine model of Hirschmann (1991) and the fcc Fe–Ni alloy model of Tomiska and Neckel (1985). If

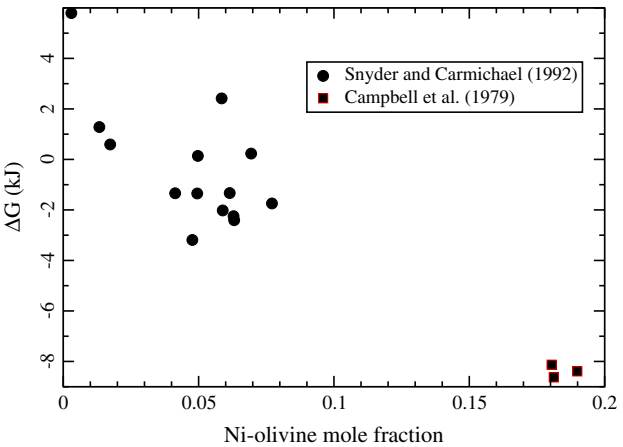

Fig. 11 Plot of ΔG for the reaction $NiSi_{0.5}O_2 + Fe \rightleftharpoons FeSi_{0.5}O_2 + Ni$ versus mole fraction Ni–olivine for experimental compositions from Snyder and Carmichael (1992) and Campbell et al. (1979) calculated using the olivine model of Hirschmann (1991) and the fcc Fe–Ni alloy model of Tomiska and Neckel (1985)

experiments are correct and thermodynamic models consistent, this value should be zero for all experiments. High-pressure olivine–alloy experiments of Seifert et al. (1988) were omitted from this plot to avoid additional errors that might be added by uncertainties in the olivine and alloy volume models. There are two important points evident from this plot. First, the errors seem to be highly correlated with X_{Ni} in the olivine (or equivalently X_{Ni} in the alloy). Second, the magnitude of these errors is similar to the apparent inconsistencies observed in the K_D^{os} plots. Ultimately, it appears that either the olivine model, solid alloy model or both will require adjustment if completely self-consistent set of olivine, alloy and sulfide models is to be achieved. Such a correction is considered beyond the scope of this study. Given the complexity of olivine relative to binary alloy, and the relative paucity of data calibrating Ni in olivine, we have chosen a final fit which most faithfully reproduces olivine-free experiments.

Barnes and Naldrett (1985) and Doyle and Naldrett (1987) suggested that low values of K_D^{os} relative to experimental values in the J-M Reef of the Stillwater Complex and similar presumably magmatic sulfide ores is a consequence of the effect of dissolved oxygen in the sulfides. They attributed this oxygen to high ambient oxygen fugacities at the time of equilibration. This interpretation was disputed by Fleet (1986), Fleet and MacRae (1987) who suggested that the low K_D^{os} are not magmatic, but instead reflect a late-stage metasomatic origin for the sulfides.

Our experiments confirm that oxygen can make up a large and variable component in the sulfide liquid under geologically reasonable conditions, particularly in iron-rich compositions. For example, O–S–Fe experiments plotted in Figs. 1 and 2 indicate oxygen contents greater than 5 mol% for experiments equilibrated 2.6 $\log_{10}$ units below FMQ. Negligible oxygen contents in Fe-rich sulfide liquids can be achieved only under quite reducing conditions.

Our thermodynamic modeling suggest that increases in oxygen content of the liquid decreases Fe-activity faster than Ni-activity, thus leading to a decrease in K_D^{os}. Furthermore, at a given oxygen fugacity, the oxygen content of sulfide liquid increases substantially with decreasing $X_{Ni}/(X_{Ni} + X_{Fe})$ in the sulfide. This supports the conclusion that low K_D^{os} values in magmatic ore deposits such as the J-M Reef reflect a combination of both high iron contents and relatively high oxygen fugacities. This interpretation is further supported by the observation that $X_{Ni}/(X_{Ni} + X_{Fe}) \approx 0.15$ in J-M Reef sulfides (Barnes and Naldrett 1985).

Conclusions

Even if copper and other components are neglected, the two-phase olivine–sulfide liquid assemblage represents a six-component system. Furthermore, sulfide oxygen and sulfur contents are almost certainly reset in any natural assemblages. Neglecting pressure for now, if one knows the cation composition of both phases, one must specify any three of the variables temperature, oxygen fugacity, sulfur fugacity and silica activity in order to estimate the fourth. K_D^{os} is, therefore, of limited usefulness in describing intensive parameters in igneous systems unless it is put in the context of equilibria with other phases such as a silicate liquid. This requires either more complicated experiments and parameterizations or accurate and self-consistent thermodynamic models for coexisting igneous phases. The thermodynamic model presented in this study represents a major step in achieving this goal.

The thermodynamic model presented in this study faithfully represents phase equilibrium and thermochemical experiments over the entire physically accessible composition space for liquids in the O–S–Fe–Ni system. In detail, the current model is a compromise between fitting K_D^{ms} experiments and K_D^{os} experiments with the metal–sulfide experiments favored. This result, along with metal–olivine Fe–Ni distribution experiments from the literature, suggest that minor adjustment is required in the mixing and/or standard-state properties for Ni–olivine in the thermodynamic model of Hirschmann (1991).

A simple thermodynamic calculator for sulfide liquids based on the model in this study will be made available through a simple web applet.[1] A more sophisticated and flexible CORBA-based interface (Kress and Ghiorso 2006) is available through the OFM Research web site.[2]

Acknowledgments Many of the experiments presented here were performed with the able help of then high school senior Mark Acton, and then undergraduate Terrie Ragins. Thanks to Mark S. Ghiorso for numerous valuable discussions and suggestions. Denton Ebel deserves sincere thanks for recognizing and publicizing inconsistencies in tabulated JANAF data. The text was substantially improved by constructive and insightful reviews by J. Brenan, D. Ebel and G. Gaetani Initial experiments in this study were performed at the Geophysical Laboratory under the NSF-sponsored Center for HIgh Pressure Research (CHIPR). Work continued under NSF grants EAR-9706786 and EAR-9980518.

References

Alfeefy HY, Lieberman JF, Stein SE, Domalski ES, Hearing ED (2001) NIST Chemistry WebBook. URL http://www.webbook.nist.gov/chemistry

Barnes SJ, Naldrett AJ (1985) Geochemistry of the J-M (Howland) Reef of the Stillwater Complex, Minneapolis Adit area. I. Sulfide chemistry and sulfide-olivine equilibrium. Econ Geol 80:627–645

[1] http://www.ctserver.ess.washington.edu/Brimstone/Brimstone-HomePage.html.

[2] http://www.ctserver.ofm-research.org/phaseProp.html.

Barnes SJ, Makovicky E, Makovicky M, Rose-Hanson J, Karup-Moller S (1997) Partition coefficients for Ni, Cu, Pd, Pt, Rh, and Ir between monosulfide solid solution and sulfide liquid and the formation of compositionally zoned Ni–Cu sulfide bodies by fractional crystallization of sulfide liquid. Can J Earth Sci 34:366–374

Boctor NZ (1981) Partitioning of nickel between olivine and iron monosulfide melts. Carnegie Inst Wash Yearb 80:356–359

Boctor NZ (1982) The effect of f_{O_2},f_{S_2} and temperature on Ni partitioning between olivine and iron sulfide melts. Carnegie Inst Wash Yearb 81:366–369

Brenan J (2003) Effects of f_{O_2},f_{S_2}, temperature, and melt composition on Fe–Ni exchange between olivine and sulfide liquid: Implications for natural olivine-sulfide assemblages. Geochim Cosmochim Acta 67:2663–2681

Brenan JM, Caciagli NC (2000) Fe–Ni exchange between olivine and sulfide liquid: Implications for oxygen barometry in sulfide-saturated magmas. Geochim Cosmochim Acta 64:307–320

Bristow CA (1939) The constitutional diagram of the alloys of iron and nickel. Part 1. The delta region. Alloy Steels Res Comm 2:1–8

Campbell IH, Naldrett AJ, Roeder PL (1979) Nickel activity in silicate liquids: some preliminary results. Can Mineral 17:495–505

Carroll MR, Rutherford MJ (1985) Sulfide and sulfate saturation in hydrous silicate melts. J Geophys Res 90:C601–C612

Cemic L, Kleppa OJ (1986) High temperature calorimetry of sulfide systems. I. Thermochemistry of liquid and solid phases of Ni + Si. Geochim Cosmochim Acta 50:1633–1641

Chase MWJ (1998) NIST-JANAF Thermochemical Tables, vol. 9 of Journal of Physical Chemistry Reference Data, 4th edn. National Institute of Standards and Technology, Washington D.C.

Chase MWJ, Davies CA, Downey JRJ, Frurip DJ, McDonald RA, Syverud AN (1985) JANAF Thermochemical Tables, vol. 14, 3rd edn. American Chemical Society, Washington, D.C.

Chuang YY, Chang YA, Schmid R, Lin JC (1986a) Magnetic contributions to the thermodynamic functions of alloys and the phase equilibria of Fe–Ni system below 1200 K. Metall Trans 17A:1361–1372

Chuang YY, Hsieh KC, Chang YA (1986b) A thermodynamic analysis of the phase equilibria of the Fe–Ni system above 1200 K. Metall Trans 17A:1373–1380

Clark T, Naldrett AJ (1972) The distribution of Fe and Ni between synthetic olivine and sulfide at 900°C. Econ Geol 67:939–952

Conard BR, McAneney TB, Sridhar R (1978) Thermodynamics of iron-nickel alloys by mass spectrometry. Metall Trans 9B:463–468

Conard BR, Meyer GA, Timberg L, Warner JS, Hynek P (1987) Thermodynamic activities of components in homogeneous Ni–Fe–S mattes at 1473–1673 K. Can Metall Q 26:299–309

Doyle CD, Naldrett AJ (1987) The oxygen content of ''sulfide'' magma and its effect on the partitioning of nickel between coexisting olivine and molten ores. Econ Geol 82:208–211

Duke JM, Naldrett AJ (1978) A numerical model of the fractionation of olivine and molten sulfide from komatiite magma. Earth Planet Sci Lett 39:255–266

Ebel DS, Grossman L (2000) Condensation in dust-enriched systems. Geochim Cosmochim Acta 64:339–366

Fincham CJB, Richardson FD (1954) The behavior of sulphur in silicate and aluminate melts. Proc R Soc Lond A 223:40–62

Fleet ME (1986) Geochemistry of the J-M (Howland) Reef of the Stillwater Complex, Minneapolis Adit area. I. Sulfide chemistry and sulfide-olivine equilibrium—a discussion. Econ Geol 81:199–203

Fleet ME (1989) Activity coefficients for FeS and NiS in monosulfide liquid and $NiSi_{1/2}O_2$ in olivine from sulfide-silicate equilibria. Geochim Cosmochim Acta 53:791–796

Fleet ME, MacRae ND (1983) Partition of Ni between olivine and sulfide and its application to Ni–Cu sulfide deposits. Contrib Mineral Petrol 83:75–81

Fleet ME, MacRae ND (1987) Partition of Ni between olivine and sulfide: the effect of temperature, f_{O_2} and f_{S_2}. Contrib Mineral Petrol 95:336–342

Fleet ME, MacRae ND (1988) Partition of Ni between olivine and sulfide: equilibria with sulfide-oxide liquids. Contrib Mineral Petrol 100:462–469

Fleet ME, MacRae ND, Herzberg CT (1977) Partition of nickel between olivine and sulfide: a test for immiscible sulfide liquids. Contrib Mineral Petrol 65:191–197

Fleet ME, MacRae ND, Osborne MD (1981) The partition of nickel between olivine, magma and immiscible sulfide liquid. Chem Geol 32:119–127

Gaetani GA, Grove TL (1997) Partitioning of moderately siderophile elements among olivine, silicate melt, and sulfide melt: constraints on core formation in the Earth and Mars. Geochim Cosmochim Acta 61:1829–1846

Gaetani G, Grove T (1999) Wetting of mantle olivine by sulfide melt: implications for Re/Os ratios in mantle peridotite and late-stage core formation. Earth Planet Sci Lett 169:147–163

Gibbs JW (1961) The Scientific Papers of J. Willard Gibbs, vol 1. Thermodynamics, vol. 1. Dover, New York

Gill PE, Murray W (1978) Algorithms for the solution fo the nonlinear least-squares problem. SIAM J Numer Anal 15:977–992

Hanson D, Freeman JR (1923) The constitution of the alloys of iron and nickel. J Iron Steel Inst 1:301–314

Hirschmann M (1991) Thermodynamics of multicomponent olivines and the solution properties of $(Ni,Mg,Fe)_2SiO_4$ and $(Ca,Mg,Fe)_2SiO_4$ olivines. Am Mineral 76:1232–1248

Katsura T, Nagashima S (1974) Solubility of sulfur in some magmas at 1 atmosphere. Geochim Cosmochim Acta 38:517–531

Kellogg HH (1976) Thermochemical modeling of molten sulfides. In: Fisher RM, Oriani RA, Turkdogan ET (eds) Physical chemistry in metallurgy: Proceedings of the Darken Conference, United States Steel, Monroeville, PA, pp 49–68

Kress VC (1997a) Magma mixing as a source for Pinatubo sulphur. Nature 389:591–593

Kress VC (1997b) Thermochemistry of sulfide liquids I: the system O–S–Fe at 1 bar. Contrib Mineral Petrol 127:176–186

Kress VC (2000) Thermochemistry of sulfide liquids II. Associated solution model for sulfide liquids in the system O–S–Fe. Contrib Mineral Petrol 139:316–325

Kress VC (2003) On the mathematics of associated solutions. Am J Sci 303:708–722

Kress VC, Ghiorso MS (2006) CTserver: a computational thermodynamics server for the geoscience community. EOS 87:V31B–0590

Kress VC, Ghiorso MS, Lastuka C (2004) Microsoft EXCEL spreadsheet-based program for calculating equilibrium gas speciation in the C–O–H–S–Cl–F system. Comput Geosci 30:211–214

Kullerud G (1961) Two-liquid field in the Fe–S system. Carnegie Inst Wash Yearb 60:174–176

Kullerud G, Yund RA (1962) The Ni–S system and related minerals. J Petrol 3:126–175

Larrain JM (1980) High temperature thermodynamic properties of iron–nickel alloys. Calphad 4:155–171

Lenz JG, Conard BR, Sridhar R, Warner JS (1978) The liquidus surface and tie-lines in the iron-nickel-sulfur system between 1473 and 1673 K. Metall Trans 9B:459–462

Li C, Naldrett A, Coats C, Johannessen P (1992) Platinum, palladium, gold, and copper-rich stringers at the Strathcona Mine, Sudbury: their enrichment by fractionation of a sulfide liquid. Econ Geol 87:1584–1598

Luhr JF (1990) Experimental phase relations of water- and sulfur-saturated arc magmas and the 1982 eruptions of El Chichón Volcano. J Petrol 5:1071–1114

Mavrogenes JA, O'Neill HSC (1999) The relative effects of pressure, temperature and oxygen fugacity on the solubility of sulfide in mafic magmas. Geochim Cosmochim Acta 63:1173–1180

Meyer GA (1972) A thermodynamic study of the systems Ni–S and Ni–Fe–S. Ph.D. Thesis, Columbia University

Meyer GA, Warner JS, Rao YK, Kellogg HH (1975) Thermodynamic properties of molten sulfides: Part 1. The system Ni–S. Metall Trans 6B:229–235

Nagamori M, Ingraham TR (1970) Thermodynamic properties of ni–s melts between 700° and 1100°c. Metall Trans 1:1821–1825

Nagashima S, Katsura T (1973) The solubility of sulfur in Na_2O–SiO_2 melts under various oxygen partial pressures at 1100°C, 1200°C, and 1300°C. Bull Chem Soc Jpn 46:3099–3103

Naldrett A, Fedorenko V, Asif M, Shushen L, Kunilov V, Stekhin A, Lightfoot P, Gorbachev N (1996) Controls on the composition of Ni-Cu sulfide deposits as illustrated by those at Noril'sk, Siberia. Econ Geol 91:751–773

O'Neill HSC, Mavrogenes JA (2002) The sulfide capacity and the sulfur content at sulfide saturation of silicate melts at 1400°C and 1 bar. J Petrol 43:1049–1087

O'Neill HSC, Pownceby MI (1993) Thermodynamic data from redox reactions at high temperatures I. An experimental and theoretical assessment of the electrochemical method using stabilized zirconia electrolytes, with revised values for the Fe–''FeO'', Co–CoO, Ni–NiO and Cu–Cu_2O oxygen buffers, and new data for the W–WO_2 buffer. Contrib Mineral Petrol 114:296–314

Peach CL, Mathez EA (1993) Sulfide melt–silicate melt distribution coefficients for nickel and iron and implications for the distribution of other chalcophile elements. Geochim Cosmochim Acta 57:3013–3021

Rammensee W, Fraser DG (1981) Activities in solid and liquid Fe–Ni and Fe–Co alloys determined by Knudsen Cell mass spectrometry. Berichte Bunsen Gesellschaft Physikalische Chemie 85:588–592

Rose L, Brenan J (2001) Wetting properties of Fe–Ni–Co–Cu–O–S melts against olivine: implications for sulfide melt mobility. Econ Geol 96:145–157

Rosenqvist T (1954) A thermodynamic study of the iron,cobalt and nickel sulfides. J Iron Steel Inst 176:37–57

Seifert S, O'Neill HSC, Brey G (1988) The partitioning of Fe, Ni and Coi between olivine, metal and basaltic liquid: an experimental and thermodynamic investigation, with application to the composition of the lunar core. Geochim Cosmochim Acta 52:603–616

Sharma RC, Chang YA (1980) Thermodynamics and phase relationships of transition metal–sulfur systems: IV. Thermodynamic properties of the Ni–S liquid phase and calculation of the Ni–S phase diagram. Metall Trans B 11B:139–146

Snyder DA, Carmichael ISE (1992) Olivine–liquid equilibria and the chemical activities of FeO, NiO, Fe_2O_3 and MgO in natural melts. Geochim Cosmochim Acta 56:303–318

Stull DR, Prophet H (1971) Janaf Thermochemical Tables, 2nd edn. National Bureau of Standards, Washington, D.C.

Thompson JBJ (1967) Thermodynamic properties of simple solutions. In: Abelson PH (ed) Researches in geochemistry, vol 2, chap 13. Wiley, New York, pp 340–361

Tomiska J (1985) Ein umgebautes massenspektrometer in kombination mit einter Knudsenzelle für thermodynamische untersuchungen bei hohen temperaturen. Das system eisen (l) - nickel(l). Zeitschrift für Metallkunde 76:532–537

Tomiska J, Neckel A (1985) Thermodynamik fester Fe–Ni Legierungen: Massenspektrometrische bestimmung der thermodynamischen mischungseffekte und berechnung des schmelzdiagramms. Berichte der Bunsen-Gesellschaft fnr Physikalische Chemie 89:1104–1109

Tsemekhman LS, Vaisburd SE (1969) Variation of the ratio Fe(III)/Fe(II) with the composition of the equilibrium metallic phase in the systems iron–nickel–oxygen and iron–cobalt–oxygen and the activity of the components. Russ J Phys Chem 43:1777–1780

Vaisburd SE, Remen TF, Scheinin AB (1969) Thermodynamic activity of iron in the system iron–nickel–sulphur at 1300°C. Russ J Phys Chem 43:1780–1781

Yoshiki-Gravelsins KS, Toguri JM (1993) Oxygen and sulfur solubilities in Ni–Fe–S–O melts. Metall Trans 24B:847–856

Zellars GR, Payne SL, Morris JP, Kipp RL (1959) The activities of iron and nickel in liquid Fe–Ni alloys. Trans Metall Soc AIME 215:181–185